RSC Advances

PAPER

Cite this: *RSC Adv.*, 2019, **9**, 40924

Visible sensing of conformational transition in model silk peptides based on a gold nanoparticles indicator†

Lan Jia, *[a] Jiabing Zhang,[b] Sumei Liu,[a] Song Chen*[a] and Jingxin Zhu [a]

Received 28th July 2019
Accepted 27th November 2019

DOI: 10.1039/c9ra05842g

rsc.li/rsc-advances

To understand protein structural transition and β-sheet formation is of importance in disparate areas such as silk protein processing and disease related β-amyloid behavior. Herein, GAGSGAGAGSGAGY (GY-14), a tetradecapeptide based on the crystallizable sequence of silk fibroin, was employed as a model peptide of the crystalline regions of silk fibroin. Due to the incorporation of tyrosine (Y), GY-14 was able to reduce Au^{3+} to Au NPs and further stabilize them without any external reducing or capping reagents to produce GY-14 stabilized Au NPs (GY-14@Au NPs). The *in situ* prepared GY-14@Au NPs were utilized as a built-in colorimetric indicator. The influences of specified physiological factors including decreasing the pH, the addition of calcium ions and isopropanol treatment on the self-assembly behavior of GY-14@Au NPs in aqueous solution have been studied. On the basis of transmission electron microscopy (TEM), dynamic light scattering (DLS), atomic force microscopy (AFM), Fourier transform infrared (FT-IR) spectroscopy and circular dichroism (CD) measurements, the color changes and the UV-Vis absorption peak shift of GY-14@Au NPs were attributed to the conformational change of the GY-14 peptide. The colorimetric readout can be seen with the naked eye, providing an efficient indicator to study the conformational changes of peptides exposed to various environmental stimuli.

1. Introduction

Protein structural transition and β-sheet formation are common phenomena both *in vivo* and *in vitro* and are of critical relevance in disparate areas such as protein processing, and β-amyloid and prion behavior.[1] The silk fibroins produced by *Bombyx mori* silkworm exist primarily in either the silk I (the silk structure before spinning) or random coil forms in the silk glands of the silkworm and undergo a conformational transition to the silk II form (the silk structure after spinning) during the spinning process.[2] The conformational analysis of silk fibroin has received considerable attention owing to its excellent mechanical property.

Many factors, such as pH,[3] metallic ions and shear force,[4] are thought to facilitate the conformation transition. A range of methods have been used to study the transition, including Fourier transform infrared (FTIR) spectroscopy,[5] Raman spectroscopy,[5–7] nuclear magnetic resonance (NMR) spectroscopy[8,9] X-ray or electronic diffraction,[10,11] scanning electron microscopy (SEM),[12,13] transmission electron microscopy (TEM),[12,14] atomic force microscopy (AFM),[15,16] circular dichroism (CD)[1,9,10] and so on. Most of the methods need sophisticated instrumentation or complicated sample preparation process. Therefore, it would be attractive if the protein conformational changes that are induced by various factors could be followed continuously and visually in time.

Gold nanoparticles (Au NPs)-based colorimetric sensing has been a subject of great interest over the past decade,[17] which takes advantage of the color change that results from the interparticle plasmon coupling during Au NPs aggregation (red to purple/blue) or redispersion of Au NP aggregates (purple to red). The colorimetric assay has been expanded for the detection of a variety of targets, including DNA,[18] proteins,[19,20] metal ions,[21] small organic compounds[22] and even whole cells.[23] Shao *et al.* reported that *in situ* prepared Au NPs could reversibly assemble/disassemble with the pH sensitive template, C12-GAGAGAGY, a peptide amphiphile.[24] Like other natural fibrous proteins, the primary structure of silk fibroin has a repetitive sequence, GAGSGA, which are able to fold into (anti-) parallel β-sheet structure in the crystalline regions of natural silk fibers.[1] Inspired by the work, we proposed that *in situ* prepared Au NPs could also serve as a visual probe for conformation transition of GAGSGA sequence in silk fibroin.

Herein, GAGSGAGAGSGAGY (GY-14), a tetradecapeptide based on the crystallizable sequence of silk fibroin, was employed as the model peptide of the crystalline regions of silk

[a]*Key Laboratory of Interface Science and Engineering in Advanced Materials, Ministry of Education, College of Material Science and Engineering, Taiyuan University of Technology, Taiyuan, 030024, P. R. China. E-mail: jialan@tyut.edu.cn*

[b]*Department Pharmacy and Machinery, China Railway 12th Bureau Group Central Hospital, Taiyuan, 030024, P. R. China*

† Electronic supplementary information (ESI) available. See DOI: 10.1039/c9ra05842g

fibroin to understand the conformation change of GAGSGA sequence in silk fibroin. Due to the incorporation of tyrosine (Y), GY-14 was able to reduce Au^{3+} to Au NPs and further stabilize them without any external reducing or capping reagents. The *in situ* prepared Au NPs could assemble simultaneously with GY-14 peptide under specified conditions such as the decreasing of the pH, the addition of calcium ions and isopropanol treatment. The conformational change of the peptide would modulate the interspaces between Au NPs. The colorimetric readout could be easily observed with the naked eye, providing an efficient probe to study conformational changes of peptide exposed to various environmental stimuli.

This proposed method has multifaceted advantages. First of all, the conformational transition of the peptide can be simply visualized by the naked eye. Second, the preparation of *in situ* Au NPs indicators is facile and low-cost. Third, the Au NPs indicator may be used in other β-sheet formation protein such as disease-related β-amyloid.

2. Materials and methods

2.1 Materials

Peptides (GY-14, GAGAGAGY (GY-8), GAGSGAGAGSGA (GS-12), 95%) were bought from GL Biochem (Shanghai) Ltd (China). $HAuCl_4 \cdot 3H_2O$ was purchased from J&K Chemical Co. (Hongkong, China). All other reagents were of analytical grade and used as received. All aqueous solutions were prepared with Mill-Q purify system.

2.2 The preparation of GY-14@Au NPs and GY-14 + cit@Au NPs

GY-14 stabilized Au NPs (GY-14@Au NPs) were prepared as follows: 100 mg peptide was dissolved in 21.72 mL NaOH aqueous solution (0.1 mol L^{-1}). Then 1 mL peptide solution was diluted by 1 mL Milli-Q water, followed by adding 2 mL $HAuCl_4$ solution (2 mM) dropwise. The molar ratio of GY-14 to Au^{3+} was 1 : 1. The pH of the mixture was adjusted to 7, and the mixture solution was stirred at 35 °C for 4 h. Then the solution was dialyzed against Mill-Q water (the pH was adjusted to 7) for 1 d.

The citrate stabilized Au NPs (cit@Au NPs) were synthesized by citrate reduction of $HAuCl_4$ as previously described.[17] GY-14 + cit@Au NPs were obtained by mixing the 500 μL as-prepared Au NP solution with 500 μL GY-14 solution (2 mM) at ambient temperature, followed by incubation for 24 h.

For the preparation of GY-8@Au NPs and GY-8 + cit@Au NPs, the procedures were the same as the preparation of GY-14@Au NPs and GY-14 + cit@Au NPs, except 100 mg GY-8 peptide was dissolved in 32.15 mL NaOH aqueous solution, and the reaction pH was adjusted to 10.

The GS-12 can not reduce the chloroauric acid by itself, the solution keep its color after 24 h at 35 °C, according to the previous report,[25] 1.0% citrate solution were added and the solution reacted at 40 °C for 2 h. The obtained Au NPs were donated as GS-12@Au NPs. GS-12 + cit@Au NPs were also made by mixing the solutions of GS-12 and cit@Au NPs.

2.3 The effect of pH, calcium ions and isopropyl alcohol

The pHs of the different series of solutions were adjusted to the desired values by addition of 1 M aqueous HCl or NaOH solutions.

Different amount of concentrated $CaCl_2$ solutions were added into the different series of solutions to obtain different final Ca^{2+} concentration (0.5 mM, 5 mM and 10 mM), the pHs were set to 7.

1 mL different series of solutions were diluted by 9 mL isopropyl alcohol, and then the mixtures were sonicated for 1 min, followed by incubation for 24 h. The final concentration of GY-14 was 0.4 mg mL^{-1}, and the pHs were set to 7.

2.4 Characterization

UV-Vis spectra were measured with a UV/Vis UV-2505 spectrometer (Shimadzu, Japan). Transmission electron microscopy (TEM) were performed on a JEM-1200EX (JEOL, Japan) operated at 80 kV. Samples of GY-14@Au NPs for TEM measurements were prepared by placing a drop of colloidal dispersion on carbon-coated copper grid, followed by evaporation of the solvent. For samples of GY-14 + cit@Au NPs and GY-14, the grids were then stained with 1 wt% phosphotungstic acid for 10 min before excess stains were blotted.

Dynamic light scattering (DLS) measurements were performed at 25 °C on a Nanotrac Wave size analyzer (Microtrac Inc., USA).

Atomic Force Microscopy (AFM) were performed on a NX10 AFM (Park Systems, Korea) with non-contact mode. 5 μL GY-14 aqueous solution was cast on silicon wafer and was allowed to dry in ambient air for 20 min. AFM scan rate was 1.0 Hz and imaging resolution was 256 × 256 pixel.

Circular dichroism (CD) measurements were performed on a MOS-500 spectropolarimeter (Bio-Logic, France) by using a quartz cell with a 1 cm path length under a nitrogen atmosphere. The spectra of sample solutions (0.1 mg mL^{-1}) were obtained from 190 to 260 nm with a 0.2 nm step and 2 s collection times per step at 20C, taking three averages.

Fourier transform infrared spectroscopy (FTIR) were obtained with a Tensor II spectrophotometer (Bruker, Germany). Samples were freeze-dried completely before being grinded into powder and pressed into pellets with KBr.

3. Results and discussion

3.1 The preparation of GY-14@Au NPs

In previous studies,[24] tyrosine was found to act as an electron donor and reduce Au^{3+} to Au^0 due to the dissociation of the phenol group of tyrosine and the relatively high oxidation–reduction potential of Au^{3+}. With the tyrosine at its C-terminal, peptide GY-14 was also speculated to have such reducing and stabilizing ability.

Fig. S1a† displayed the time-resolved UV absorption of the $HAuCl_4$/GY-14 mixture without addition of any other reducing or stabilizing reagents. A new peak immediately appeared around 520 nm after adding $HAuCl_4$ to GY-14 solution, indicating the formation of Au NPs with particle size less than

20 nm.[24] This band was weak and broad at the beginning and then gradually turned to intensive and sharp. Its maximum absorption was reached after 210 min post-mixing, suggesting the complete *in situ* reduction of Au^{3+}. Meanwhile, the color of the solution changed from yellow to red. TEM images confirmed the formation of spherical Au NPs with an average diameter of 16.2 ± 6.9 nm (Fig. S1b†), which was consistent with the estimation from UV spectra.

In order to understand the role of tyrosine residue in the reduction of Au^{3+}, UV-Vis absorption spectra of the GY-14 were measured before and after the reduction process. As shown in Fig. S2,† the strong absorption band at *ca.* 275 nm due to the π–π* transition of tyrosine residue in GY-14 got smaller and eventually vanished, indicating that the tyrosine residue played some role in this reduction process. Since no additional capping reagents were added, it was possible that the formed AuNPs were stabilized by the carboxyl groups of the GY-14 at pH 7, the steric hindrance might also play some role in the stabilization.

As the colorimetric indicator, the *in situ* prepared Au NPs should assemble with the peptide without disturbing the conformation change of the peptide apparently, two control groups were utilized in the system, one group was GY-14 + cit@Au NPs and used to demonstrate the role of the *in situ* prepared Au NPs; the other one was GY-14 itself and used to clarify the effect of the Au NPs on assembly behavior of the peptide.

3.2 The effect of pH

It is known that pH is thought to be important factor in affecting conformations of silk fibroin in the natural spinning process,[26] which may also affect the conformation of GY-14. Fig. 1 displayed the UV-Vis spectra of GY-14@Au NPs and GY-14 + cit@Au NPs at different pH conditions.

The GY-14@Au NPs solutions in Fig. 1a showed nearly no obvious color change at different pH, whereas the GY-14 + cit@Au NPs solutions in Fig. 1b expressed obvious color variation around pH 4. The GY-14 + cit@Au NPs at low pH became more dilute over time and the color changed from wine red to light purple after 24 h. Correspondingly, the SPR band almost vanished, which was associated with aggregation of Au NPs. The peptide was negatively charged due to the dissociated carboxyl group at neutral or alkaline condition. When the pH decreased to 4, the dissociated carboxyl groups were gradually protonated, resulting in the elimination of electrostatic repulsion. The stabilization mechanism of peptide for the NPs was the same as the citrate. The result was in accordance with previous results on the precipitation of Au NPs obtained by citrate reduction routes upon the change in pH.[17] The phenomenon was not the same for the *in situ* prepared Au NPs, the absorption peak of GY-14@Au NPs red shifted from 520 nm to 523 nm as the pH decreased from 7 to 4, with peak broadening and intensity decreasing. It was supposed that these Au NPs might be assembled with the peptide, resulting in the change of the interparticle distance and the red-shift of the plasmon peak.

The effect of changing pH in GY-14@Au NPs and GY+14@Au NPs have been investigated respectively. By adjusting the pH value of the GY-14@AuNPs solution after 24 h incubation from 4 back to 7, the λ_{max} shifted from 523 nm to around 516 nm, accompanied by the peak narrowing and intensity increasing (Fig. S3a†). The GY-14@AuNPs can keep stable at pH 4 at least for one month, and the reverse procedure could be repeated for many times. The result indicated that the conformation transition under different pH were reversible.

The GY-14 + cit@Au NPs did not exhibit the same degree of reversibility. As the solution became unstable after 24 incubation at pH 4, the pH was adjusted from 4 to 7 after 6 h incubation. As shown in Fig. S3b,† the λ_{max} of 525 nm at pH 7 shifted to around 600 nm at pH 4. Then the pH was reversibly adjusted to 7, the λ_{max} shifted to around 535 nm with significant decreased intensity. Also the color only partially returned its original red color, retaining a slight blue character.

To clarify the role of peptide sequence, two control peptides were introduced. The one is octapeptide GAGAGAGY (GY-8), which has the tyrosine residues but will not undergo conformation change under acidic acid. Another one is dodecapeptide GAGSGAGAGSGA (GS-12), which is from the crystalline region without tyrosine moiety. For GY-8@Au NPs, when the pH was adjusted to 4, the color turned blue quickly and the Au NPs aggregated and settled to the bottom after 2 h (Fig. S4a†). The GY-8 + cit@Au NPs were also not stable under acidic pH, the

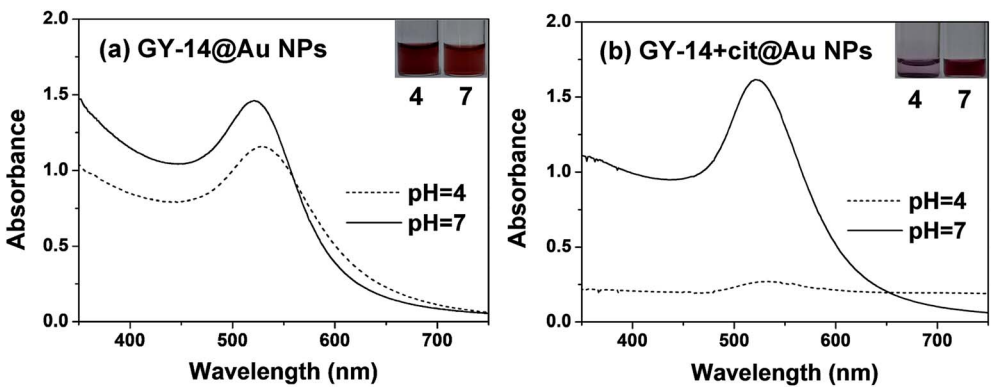

Fig. 1 The UV-Vis spectra of (a) GY-14@Au NPs and (b) GY-14 + cit@Au NPs after 24 h at different pH conditions.

λ_{max} shifted from 527 nm to 565 nm with the peak broadening, the color changed from red to purple (Fig. S4b†).

For GS-12@Au NPs, GS-12 could not reduce Au^{3+} to Au^0 as the color of solution did not change after 24 h when the solution contained only GS-12 and $HAuCl_4$, then citrate was added as the reducing agent. The color of GS-12@Au NPs solution changed to blue quickly, and the solution became transparent as the precipitation settled after 24 h, the λ_{max} shifted from 528 nm to 550 nm in the UV-Vis spectra (Fig. S5a†). For GS-12 + cit@Au NPs, the similar phenomenon can be observed. The color converted form red to light blue, and the peak intensity decreased significantly (Fig. S5b†). From the TEM image, some Au NPs distributed along the peptide strips at pH 4 (Fig. S6a†), while others distributed randomly. It might be ascribed to the interaction between the serine residue in GS-12 and Au NPs. After 24 h, both of GS-12@Au NPs and GS-12 + cit@Au NPs were precipitated with almost transparent solutions. From the results of the two control peptide, the tyrosine moiety was essential for the reduction of Au NPs, and the crystallizable sequence was very important for conformation transition.

The assembly of GY-14@Au NPs at low pH was further supported by TEM images. At pH 4, the distribution of GY-14@Au NPs along the peptide strips was visualized (Fig. 2a), causing a "stain" effect on the peptide assemblies. At pH 7, the GY-14@Au NPs were well dispersed, and the peptide could not be observed without staining (Fig. 2d). These particles got much closer at pH 4 than the ones at pH 7, in accordance with the UV-Vis spectra. The GY-14 + cit@Au NPs indeed aggregated at pH 4, and the aggregated Au NPs were isolated from the peptide (indicated by red arrow in Fig. 2b). At pH 7, it was seemed that GY-14 peptide formed bead-like structure; the Au NPs were dispersed randomly (Fig. 2e).

We also investigated the morphology of GY-14 at different pH conditions. The GY-14 was found to self-assemble at pH 4. TEM image showed that the rod-like strips with several hundreds of nanometers to several micrometers in length developed from the aqueous solution (Fig. 2c). AFM images of GY-14 showed more clear morphology. From the concentration of 0.05 mg mL^{-1}, the longer strips composed of segmented structures and bead-like structures were observed at pH 4 (Fig. S7a†), which implied that the bead-like oligomers might self-assemble into protobrils. By the cross section analysis, the height of the strips was around 3 nm (Fig. S7c†), which was consistent with previous reports.[27] At pH 7, the globule-like structures with different sizes could be seen in the images (Fig. S7b†), and the morphology was similar to that in the Fig. 2f.

DLS experiments were conducted to further study the size distribution of GY-14@Au NPs, GY-14 + cit@Au NPs and GY-14 at different pH condition. As shown in Fig. 3, at pH 4.0, after incubation for 3 days at room temperature, GY-14@Au NPs exhibited a quite broad size distribution from 200–1000 nm, the hydrodynamic diameter was around 500 nm. The GY-14 showed two peaks around 500 nm and 1000 nm, respectively. The size of GY-14 + cit@Au NPs was smaller than the other two samples, as GY-14 + cit@Au NPs would form precipitation after 3 days, so

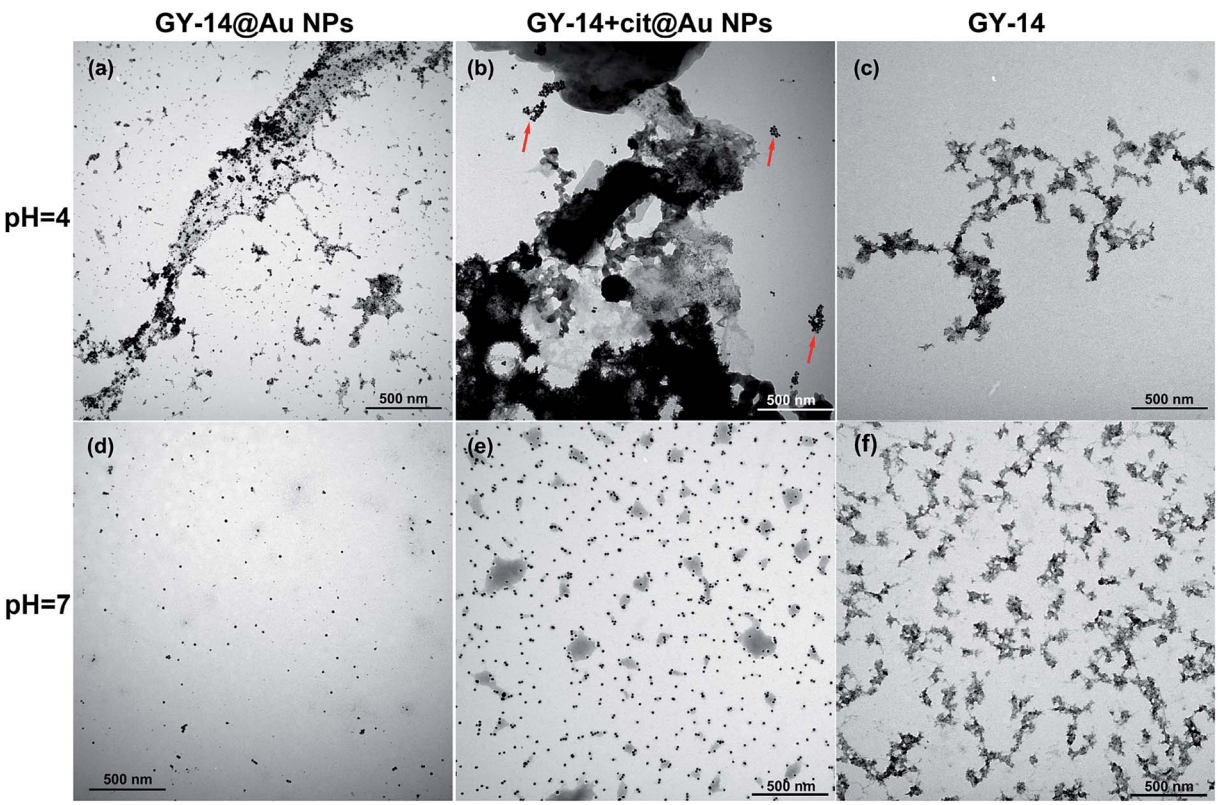

Fig. 2 The TEM images of GY-14@Au NPs (a) and (d), GY-14 + cit@Au NPs (b) and (e) and GY-14 (c) and (f) at different pH conditions.

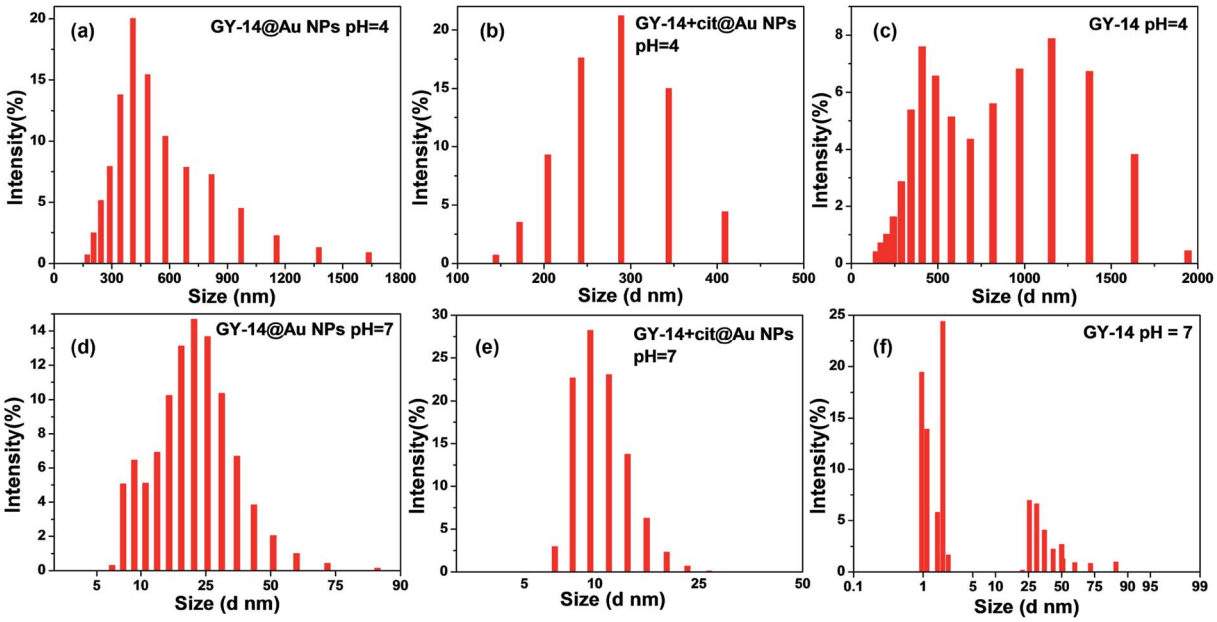

Fig. 3 DLS data of GY-14@Au NPs (a) and (d), GY-14 + cit@Au NPs (b) and (e) and GY-14 (c) and (f) at different pH conditions.

this sample was tested after 6 h incubation. Time might be too short for the peptide to assembly. At pH 7, all the three samples had much narrow size distribution, and the hydrodynamic diameters were less than 100 nm. The DLS results were basically agreed with the TEM measurements.

To characterize the structure of the peptide, the FTIR and CD spectra at different pH were also examined. The FTIR spectrum of the GY-14@Au NPs showed that the amide I band 1646 cm^{-1} at pH 7, which was usually indicative of a random coil structure.[28] When pH decreased to 4, a new band 1677 cm^{-1} appeared, which indicated the presence of β-sheet structure. Circular dichroism (CD) spectra of CY-14@Au NPs at pH 7 showed characteristic negative band at 195 nm, which supported random coil form of GY-14 (Fig. 4b). When adjusting pH to 4, the negative band reversed, indicating the conformation transition from random coil to β-sheet (Fig. 4b). The FTIR and CD spectra of GY-14 under different pH presented the similar results (Fig. S8†).

It is noticeable, however, that the formed β-sheet structure is not perfect antiparallel β-sheet structure. The tyrosine moiety might hinder the β-sheet transition due to the steric effect of the big aromatic ring. At lower pH, the peptide GY-14 exhibited a tendency to aggregate into β-sheet conformation, spontaneously driving the Au NPs to assembly along the strips. The co-assembly of the *in situ* Au NPs could be observed visually by the color change, as well as the peak shift in UV-Vis spectra.

3.3 Effect of Ca^{2+} ions

It is known the metal ions (for example, Na^{+}, K^{+}, Ca^{2+}, Cu^{2+}, Mg^{2+}) can affect the formation of silk fibroin solution along the secretory pathway of silkworm and the subsequent spinning process.[29] As K and Ca were the most abundant elements in the gland. Ca^{2+} ion was chosen as the representative ion as the effect of Ca was found to be more evident.

As shown in Fig. 5a, with the increasing concentration of Ca^{2+} ions from 0.5 mM to 10 mM, the absorption peak of GY-

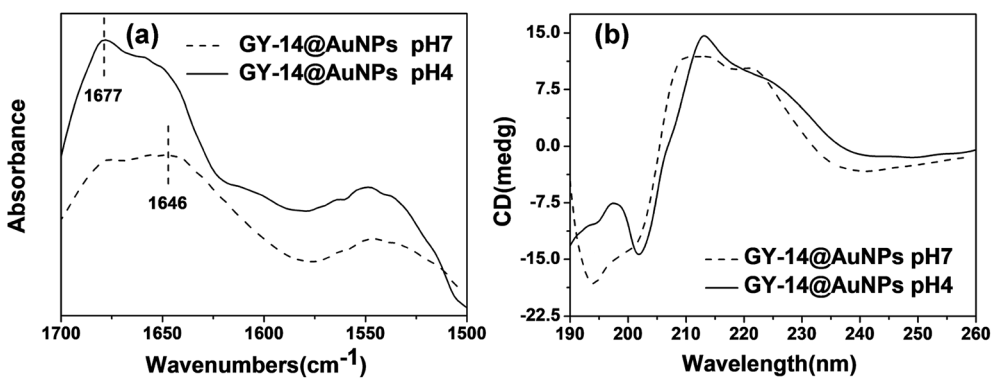

Fig. 4 FTIR spectra (a) and circular dichroism spectra (b) of GY-14@Au NPs under different pH conditions.

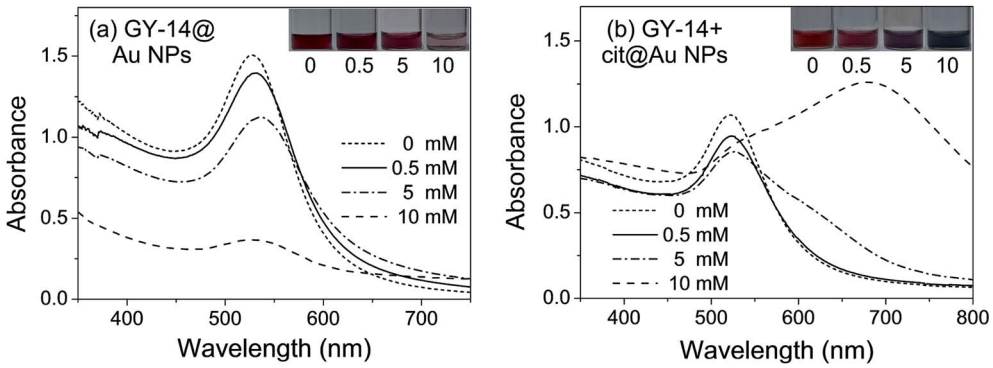

Fig. 5 The UV-Vis spectra of (a) GY-14@Au NPs, (b) GY-14 + cit@Au NPs with different concentrations of Ca^{2+} ions.

14@Au NPs red shifted from 528 nm to 536 nm, accompanying with the peak broadening and the intensity decreasing, especially with 10 mM Ca^{2+} ions. In addition, the color became light pink when the concentration of Ca^{2+} ions reached 10 mM. For the GY-14 + cit@Au NPs system, the color rapidly changed from red to purple and blue with 5 mM and 10 mM Ca^{2+} ions, respectively. The absorption peak even red shifted to ~675 nm with 10 mM Ca^{2+} ions, which indicated the particle aggregation.

As demonstrated by TEM images, with the increasing of Ca^{2+}, the assemble behavior of *in situ* prepared Au NPs along the peptide assemble structure became more evident. It was found at lower Ca^{2+} ions concentration, for example, 0.5 mM, only small part of the Au NPs began to distribute along the peptide, then the trend became evident with 5 mM Ca^{2+} ions, and most of the Au NPs spread along the peptide strips with 10 mM Ca^{2+} ions, also the peptide strips grew bigger with high Ca^{2+} ion concentration. While in GY-14 + cit@Au NPs system, the assembly for Au NPs that array on the peptide strips could rarely be observed, the aggregate of Au NPs were separated from the staining peptide (Fig. 6c, indicated by the red arrows). The GY-14 itself was assembled with 10 mM Ca^{2+} ions, and the strips were composed of bead-like structure, with diameters of the bead in the range of 50–100 nm. This morphology was frequently demonstrated in other reports.[30–32] Also, the AFM images showed the fibrous and bead-like structures (Fig. S9†).

The FT-IR results also verified the tendency of conformation transition (Fig. 7a). The GY-14@Au NPs showed the characteristic amid I peak at 1662 cm^{-1} (with 0.5 mM Ca^{2+}) and 1658 cm^{-1} (with 5 mM Ca^{2+}), these two amide I peaks probably corresponded to β-turns and bends. When the concentration of Ca^{2+} increased to 10 mM, the spectra of GY-14@Au NPs showed the characteristic amid I peak 1643 and 1679 cm^{-1}, the latter one indicated the presence of β-sheet structure. In addition, as shown in Fig. 7b, with 0.5 mM Ca^{2+}, CD spectra of GY-14@Au NPs demonstrated a strong negative band centered around 194 nm and a positive band around 212 nm, indicating the dominance of random-coil structure. However, when the Ca^{2+} concentration increased to 10 mM, the two bands drastically inverted to a positive band at ~196 nm and to a negative band at ~215 nm, showing the emerge of β-sheet conformation. CD spectra revealed that the GY-14@Au NPs solution experienced a gradual conformation change from a typical random coil to β-sheet with the increasing of Ca^{2+} concentrations. The FTIR and CD spectra of GY-14 itself with different concentration of Ca^{2+} appeared the similar trends (Fig. S10†).

Previously reports revealed that Ca^{2+} played a significant role in the formation of silk. Magoshi *et al.* proposed that Ca^{2+} ions favor the gelation and stable storage of the liquid silk gel in silk gland lumen.[33] Zhou *et al.* showed that at lower pH (5.2) and a certain amount of Ca^{2+} ions (10 mg per gram of fibroin) favored the formation of silk II, while higher pH (6.9–8.0) and higher Ca^{2+} ions concentrations maintain "random coil" conformation typical of silk I.[34] Shao *et al.* found that as the concentration of Ca^{2+} increased in the regenerated silk fibroin (RSF) aqueous solutions, the conformational transition to β-sheet was promoted.[35] In our system, it was found that β-sheet was promoted with increasing concentration of Ca^{2+} ions. The peptide model is quite different from the RSF. This implied that the action mechanism of Ca^{2+} ions in the RSF system might be inapplicable to the peptide system. It was supposed that Ca^{2+} ions might bind to the peptide with repetitive –GAGAGS–, causing it to adopt a β-sheet conformation.

3.4 Effect of isopropanol

It is reported the solvent played important role in conformation transition of silk fibroin.[36] Alcohol treatment is mostly commonly method used to trigger the transition from silk I to silk II. Methanol and ethanol have been carefully investigated. Isopropanol treatment demonstrated a relative slow β-sheet formation process compared with methanol and ethanol. Isopropanol was chosen in our system to get a moderate transition rate for easy observation.[37] 90% isopropanol solution was used as it was reported that conformation transition of silk fibroin induced by isopropanol solutions of high concentrations.[38]

Fig. 8 displayed the UV-Vis spectra of GY-14@Au NPs and GY-14 + cit@Au NPs with isopropanol. The color of the GY-14 + cit@Au NPs immediately turned blue upon the addition of isopropanol, accompanied by the floccules, and the absorption peak almost vanished in the spectrum. In contrast, the color of GY-14@Au NPs became purple red with an absorption peak at around 550 nm within seconds.

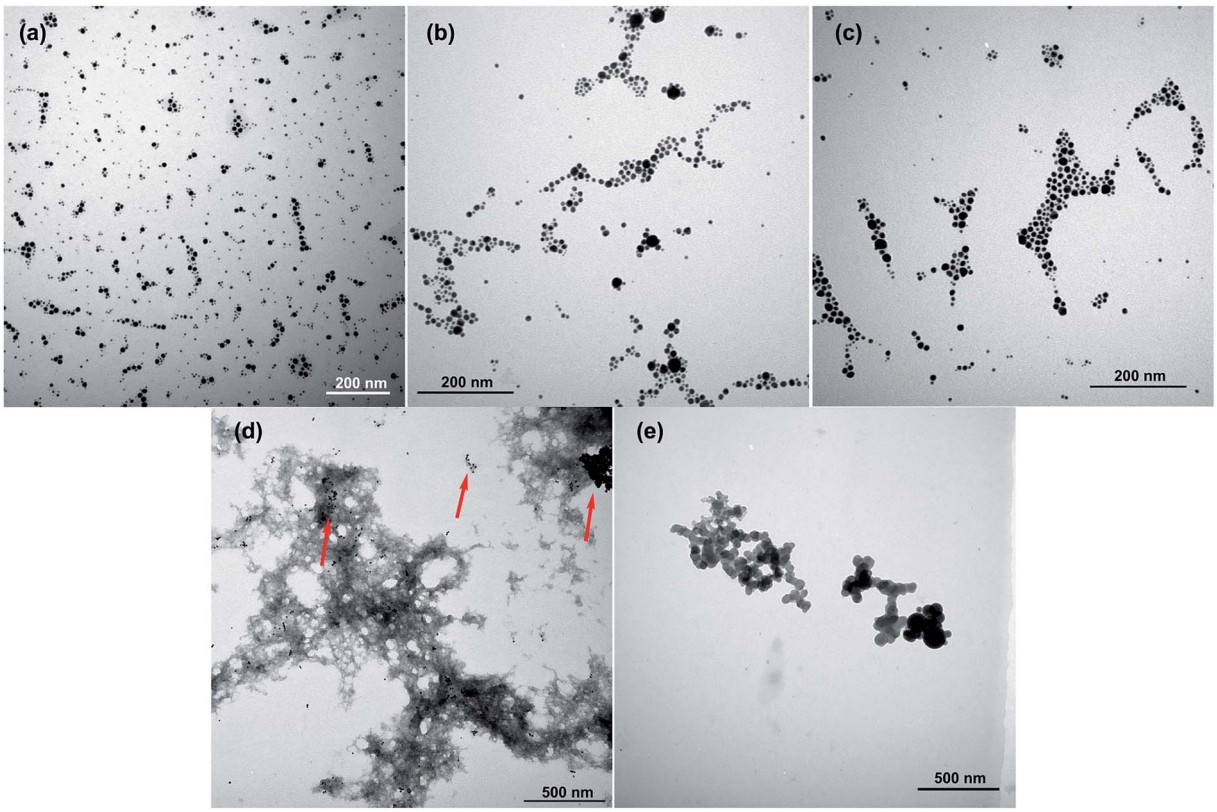

Fig. 6 The TEM images of GY-14@Au NPs with (a) 0.5 mM, (b) 5 mM and (c) 10 mM Ca^{2+} ions; (d) GY-14 + cit@Au NPs with 10 mM Ca^{2+} ions and (e) GY-14 with 10 mM Ca^{2+} ions.

The assembly morphology of the GY-14 after isopropanol treatment was investigated by TEM machine. As shown in Fig. 9, most of the *in situ* prepared Au NPs arrayed on the fibrous peptide (Fig. 9a), while the GY-14 + cit@Au NPs aggregations were separated from the peptide (Fig. 9b, indicated by the red arrows). Also, the TEM and AFM images of GY-14 itself showed fibril assemblies (Fig. 9c and S11†). Similarly, it was found the fibril assemblies exhibited a "beads on a string" type of morphology, with height about 3 nm in the magnified AFM images (Fig. S11†). The FTIR spectrum of GY-14@Au NPs also indicated the β-sheet conformation, where the amide I band located around 1678 cm^{-1} after isopropanol treatment.

The mechanism of the conformation transition after isopropanol treatment was similar to that of the methanol and ethanol. According to the literature,[39] when a hydrophilic alcohol was added to the silk fibroin or GY-14 peptide solution, the molecular chain interacted quickly and strongly with one another, and then the chains were rearranged in a regular array to some extent, which changed the conformation from a random coil to a β-sheet structure.

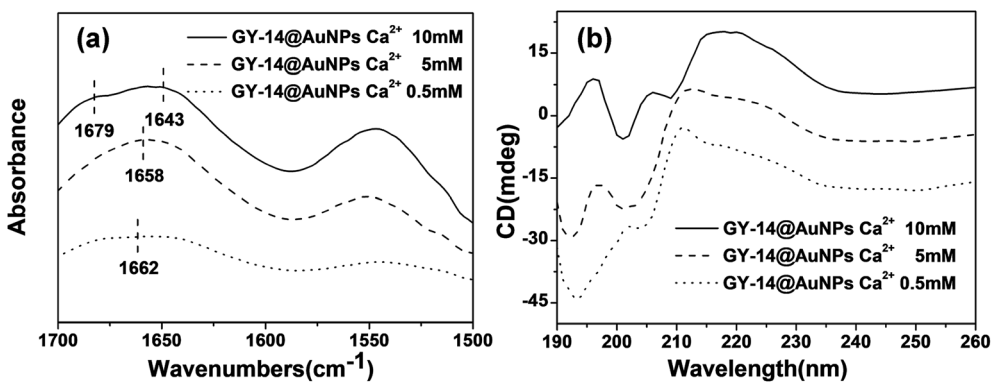

Fig. 7 FTIR spectra (a) and circular dichroism spectra (b) of GY-14@Au NPs with different concentration of Ca^{2+}.

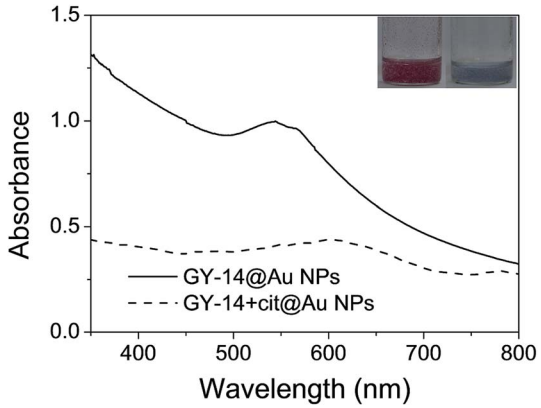

Fig. 8 The UV-Vis spectra of GY-14 + cit@Au NPs and GY-14@Au NPs with isopropanol solution (90%).

The Au NPs indicator can follow peptide conformational changes continuously and visually in time with the color change, and the UV-Vis absorption spectra serve to measure the extent of conformational change for different solution conditions. Among the three influence factors, pH played minor role as the changes of the color and the absorption peak were not significant. However, the effect of isopropanol treatment was obvious, the color changed immediately and the peak shifted dramatically. As the conformation transition is concentration dependent, more elaborate results might be obtained by varying the concentrations of peptide. Also, the indicator may provide a practical reliable and rapid sample screen method as the status of the samples can be predicated.

4. Conclusion

We have described the possibility of using Au NPs as a colorimetric sensor for model peptide conformation transition under specified conditions. Upon exposed to different environments, including lower pH, a certain amount of Ca^{2+} ions (>5 mM) and isopropanol (90%) treatment, the peptide have a tendency to aggregate into β-sheet. The conformational change of the peptide modulates the interspaces between Au NPs and causes visible color change of the *in situ* prepared Au NPs solution. On the basis of TEM, DLS, FI-IR and CD measurements, the color changes of the Au NPs and the shift of the adsorption peak in UV-Vis spectra were ascribed to the conformational transition of the peptide. The Au NPs can easily and reliably be used to create a simple and inexpensive probe for peptide or even protein

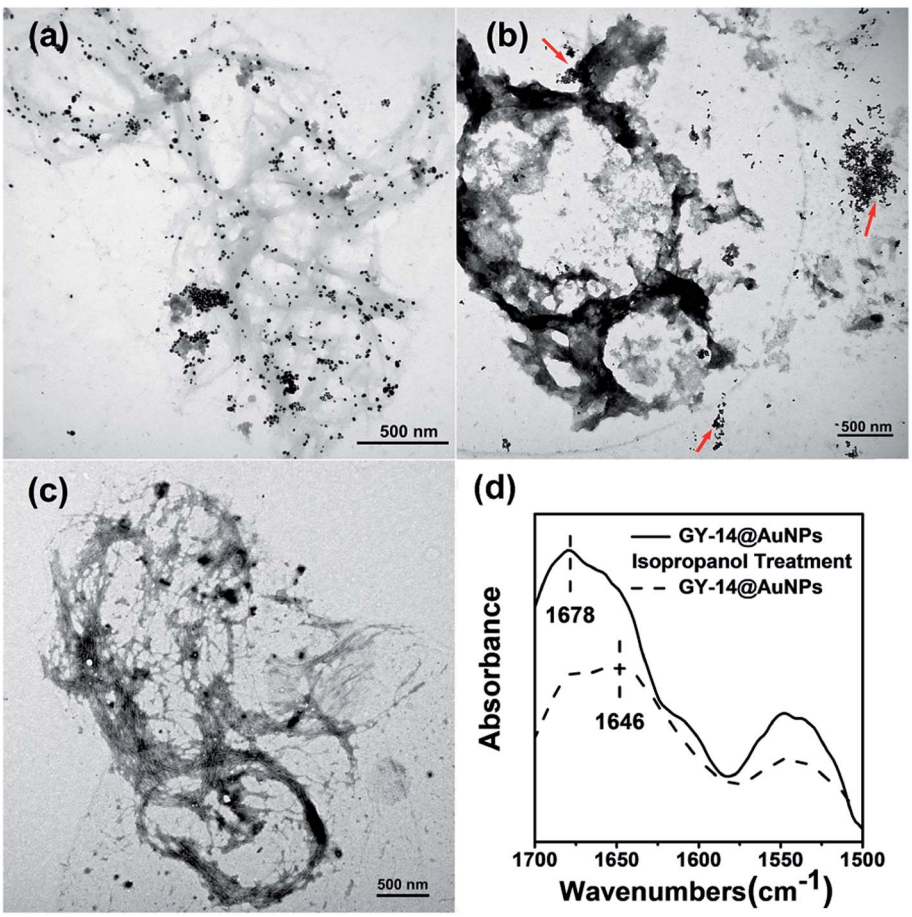

Fig. 9 The TEM images of (a) GY-14@Au NPs, (b) GY-14 + cit@Au NPs, (c) GY-14 and (d) FT-IR spectra of GY-14@Au NPs and GY-14@Au NPs with isopropanol solution (90%).

conformation change. The method also has practical implication as a reliable and rapid sample selection strategy.

Conflicts of interest

There are no conflicts to declare.

Acknowledgements

We gratefully acknowledge the financial support from the National Nature Science Foundation of China (Grant No. 51303124) and Natural Science Foundation of Shanxi province (Grant No. 201801D121360 and 201801D121102).

References

1 R. V. Donna Wilson and D. Kaplan, *Biophys. J.*, 2000, **78**, 2690–2701.
2 T. Asakura and D. L. Kaplan, *Encyclopedia of Agricultural Science*, 1994, vol. 4, p. 1.
3 C. Tallian, A. Herrero-Rollett, K. Stadler, R. Vielnascher, K. Wieland, A. M. Weihs, A. Pellis, A. H. Teuschl, B. Lendl, H. Amenitsch and G. M. Guebitz, *Eur. J. Pharm. Biopharm.*, 2018, **133**, 176–187.
4 Y. Zhang, Y. Zuo, S. Wen, Y. Hu and Y. Min, *Biomacromolecules*, 2018, **19**, 1223–1233.
5 J. Z. Shao, J. H. Zheng, J. Q. Liu and C. M. Carr, *J. Appl. Polym. Sci.*, 2005, **96**, 1999–2004.
6 G. F. P. Monti, A. Bertoluzza, N. Kasai and M. Tsukada, *J. Raman Spectrosc.*, 1998, **29**, 297–304.
7 P. T. P. Monti, G. Freddi, T. Asakura and M. Tsukada, *J. Raman Spectrosc.*, 2001, **32**, 103–107.
8 D. Tian, T. Li, R. Zhang, Q. Wu, T. Chen, P. Sun and A. Ramamoorthy, *J. Phys. Chem. B*, 2017, **121**, 6108–6116.
9 S. W. Ha, T. Asakura and R. Kishore, *Biomacromolecules*, 2006, **7**, 18–23.
10 A. Seves, M. Canetti, F. Secundo and G. Vecchio, *Biopolymers*, 1989, **28**, 1613–1624.
11 M. Muller, C. Riekel and F. Vollrath, *Macromolecules*, 1999, **32**, 4464–4466.
12 P. Chen, H. S. Kim, C.-Y. Park, H.-S. Kim, I.-J. Chin and H.-J. Jin, *Macromol. Res.*, 2008, **16**, 539–543.
13 A. Matsumoto, A. Lindsay, B. Abedian and D. L. Kaplan, *Macromol. Biosci.*, 2008, **8**, 1006–1018.
14 Z. G. Gong, L. Huang, Y. H. Yang, X. Chen and Z. Z. Shao, *Chem. Commun.*, 2009, 7506–7508, DOI: 10.1039/b914218e.
15 I. Greving, M. Cai, F. Vollrath and H. C. Schniepp, *Biomacromolecules*, 2012, **13**, 676–682.
16 J. Zhong, X. Liu, D. Wei, J. Yan, P. Wang, G. Sun and D. He, *Int. J. Biol. Macromol.*, 2015, **76**, 195–202.
17 K. Saha, S. S. Agasti, C. Kim, X. Li and V. M. Rotello, *Chem. Rev.*, 2012, **112**, 2739–2779.
18 L. M. Zanoli, R. D'Agata and G. Spoto, *Anal. Bioanal. Chem.*, 2012, **402**, 1759–1771.
19 S. Chah, M. R. Hammond and R. N. Zare, *Chem. Biol.*, 2005, **12**, 323–328.
20 H.-J. Zhang, H.-Z. Zheng, Y.-J. Long, G.-F. Xiao, L.-Y. Zhang, Q.-L. Wang, M. Gao and W.-J. Bai, *Talanta*, 2012, **89**, 401–406.
21 D. Li, A. Wieckowska and I. Willner, *Angew. Chem., Int. Ed.*, 2008, **47**, 3927–3931.
22 J. S. Lee, P. A. Ulmann, M. S. Han and C. A. Mirkin, *Nano Lett.*, 2008, **8**, 529–533.
23 C. D. Medley, J. E. Smith, Z. Tang, Y. Wu, S. Bamrungsap and W. Tan, *Anal. Chem.*, 2008, **80**, 1067–1072.
24 J. Zhang, T. Xu, J. Yao, L. Huang, X. Chen and Z. Shao, *RSC Adv.*, 2012, **2**, 5599–5604.
25 M. C. Daniel and D. Astruc, *Chem. Rev.*, 2004, **104**(1), 293–346.
26 J. Zhu, Y. Zhang, H. Shao and X. Hu, *Polymer*, 2008, **49**, 2880–2885.
27 J. Zhong, M. Ma, W. Li, J. Zhou, Z. Yan and D. He, *Biopolymers*, 2014, **101**, 1181–1192.
28 N. N. Kalnin and S. Y. Venyaminov, *Biopolymers*, 1990, **30**, 1259–1271.
29 X. C. L. Zhou, Z. Z. Shao, Y. F. Huang and D. P. Knight, *J. Phys. Chem. B*, 2005, **109**, 16937–16945.
30 Y. X. He, N. N. Zhang, W. F. Li, N. Jia, B. Y. Chen, K. Zhou, J. H. Zhang, Y. X. Chen and C. Z. Zhou, *J. Mol. Biol.*, 2012, **418**, 197–207.
31 S. Bai, S. Liu, C. Zhang, W. Xu, Q. Lu, H. Han, D. L. Kaplan and H. Zhu, *Acta Biomater.*, 2013, **9**, 7806–7813.
32 Y. Z. Chen, C. K. Tang, Z. H. Xing, J. Zhang and F. Qiu, *J. Pept. Sci.*, 2013, **19**, 708–716.
33 Y. M. J. Magoshi, M. Kato, M. A. Becker and S. Nakamura, *Abstracts of Papers of the American Chemical Society*, 1997, **214**, 209.
34 X. X. P. Zhou, D. P. Knight, X. H. Zong, F. Deng and W. H. Yao, *Biochemistry*, 2004, **43**, 11302–11311.
35 Y. Jin, Y. C. Hang, Y. P. Zhang, H. L. Shao and X. C. Hu, *Mater. Res. Innovations*, 2014, **18**, 113–116.
36 B. Q. Zuo, L. Liu and Z. Wu, *J. Appl. Polym. Sci.*, 2007, **106**, 53–59.
37 N. Goujon, R. Rajkhowa, X. G. Wang and N. Byrne, *J. Appl. Polym. Sci.*, 2012, **6**, 4411–4416.
38 L. Z. X. Chen, Z. Z. Shao, P. Zhou, D. P. Knight and V. Fritz, *Acta Chim. Sin.*, 2003, **61**, 625–629.
39 Y. H. P. J. Nam, *J. Appl. Polym. Sci.*, 2001, **81**, 3008–3021.

